Effect of temperature on structural and optical properties of Sm_2O_3

B Bharati[1,2], P Mohanty[2], B Sondezi[2] and S Sitha[1]

[1]Department of Chemical Sciences, University of Johannesburg, P.O. Box 524, Auckland Park, Johannesburg 2006, South Africa
[2]Department of Physics, University of Johannesburg, P.O. Box 524, Auckland Park, Johannesburg 2006, South Africa

E-mail: bharatib@uj.ac.za,bharatib47@gmail.com

Abstract. In this work, the Sm_2O_3 sample was synthesized through the sol-gel technique. It has then been focused on how the calcination temperature affects the structural and photocatalytic properties of the material. Therefore, the synthesized powder sample has been calcined at two different temperatures, which are 500 and 700 ˚C. The structural and optical properties, along with photocatalytic properties, have been studied. The structural analysis through x-ray diffraction (XRD) confirmed that the compounds crystallize in a cubic structure with a lattice parameter, *a*, is 10.94 Å. The crystallite size calculated from the XRD data is 16 nm for the 500 ˚C calcined sample and 23 nm for the 700 ˚C calcined sample. Fourier transform infrared (FTIR) spectra have demonstrated the presence of Sm-O stretching vibrations in both of the synthesized samples. The photocatalytic performance of both samples was examined by degrading the Methylene Blue (MB) dye with irradiation of UV light and found that the sample calcined at 700 ˚C is more efficient compared to the 500 ˚C calcined sample.

1 Introduction

In recent times, metal oxides are used in several areas and particularly a number of research events have been commenced to explore rare-earth metal oxides. Metal oxides are prevalent because of their irreplaceable properties. A sequence of rare-earth-metal-based compounds is widely used in numerous fields of existing science and technology due to the outcome of its infrequent optical, chemical, magnetic, electrical and catalytic properties arising from its distinctive 4*f* electrons [1, 2]. The rare earth metal oxides are extensively useful in the arenas of biochemical probes, optical transmission, luminescence devices, medical diagnostics, etc [3]. These rare-earth metal oxide compounds are the most stable rare-earth compounds with the rare-earth ions left behind in the trivalent state [3]. It is known that R_2O_3 nanocompounds display better catalytic and luminescence properties [3]. Lanthanides' rare earth metal compounds are extensively used in numerous fields of current science and technology [2]. It has been widely used in nano sensors, photoelectronics, and micro-circuit batteries, which has aroused considerable interest over the past several years [1]. The usage of a metal oxide as a photocatalyst is very common for the humiliation of organic contaminants [2, 4-13]. The fabric manufacturing enterprises produce so much wastewater, which comprises with abundance of organic pollutants [14]. The contaminants create problems in the ecosystem due to their unchanging chemical nature, posing numerous mutagenic and carcinogenic risks [2]. Because of this existing risk, wastewater treatment is one of the all times attracted technical field. The heterogeneous photocatalysis process, which comprises with

advanced oxidation process (AOP), delivers the consequence for the degradation of organic pollutants in wastewater [2, 4-13]. This degradation process of the AOP encompasses the creation of superoxide ($\cdot O_2^-$) radicals and hydroxyl ($\cdot$OH) radicals [5]. These two radical species are unsteady and therefore attack organic contaminants and create non-harmful products which are biocompatible [2, 4-13]

Rare earth metals are used in a wide range of applications, such as ultraviolet (UV) detectors, high-resolution x-ray imaging, catalysts and fluorescent materials, owing to their high chemical stability and UV absorption capability [2]. Lanthanide rare earth metal compounds are nowadays being used in photocatalysis, owing to their exceptional *f*-electronic arrangement [2]. The Nanoparticles are very small units that exist in the range of 1-100 nm, in which substantial quantities of atoms are situated in the interfacial region in a disorderly fashion, resulting in unusual physical and chemical properties [3, 12, 13, 15]. Therefore, rare earth metal oxide nanoparticles are the most attractive materials for photocatalysis [2, 4-11]. Recently, a few reports have studied the photocatalytic properties of rare-earth metal oxide nanoparticles [2, 4-11]. Sm_2O_3 is a species of encouraging rare earth oxide functional materials in recent times because of its wide energy gap, high electrical resistivity, high dielectric constant and better chemical and thermal stability [16-19]. However, in this report, Sm_2O_3 nanoparticles have been synthesized. Further, the effect of calcination temperature on the structural and photocatalytic properties of the Sm_2O_3 sample has been studied.

2 Experimental details

Sm_2O_3 sample was synthesized through the sol-gel method [12, 13]. For the synthesis of Sm_2O_3 at first $Sm(NO_3)_3$ and ethanol were mixed to make the solution. With the help of a magnetic stirrer, the prepared solution of the precursors was stirred for 3 h. Then the solution was kept for 24 h for aging. After aging, the liquid was heated to dry to get the solid sample. After drying, the solid sample was crushed into powder. The powdered sample was then calcined at 500 and 700 ºC for three hours in a box furnace. The prepared sample was used for characterization, using X-ray diffraction (XRD) technique with Cu-*K*α radiation (λ = 1.5406 Å), and Fourier transform infrared (FTIR) spectra. Then, the photocatalysis measurements of the samples were carried out by degrading the dye methylene blue (MB) with irradiation of UV light. Further, in this report, the samples calcined at 500 and 700 ˚C are referred to as Sm_2O_3-500 and Sm_2O_3-700, respectively.

3 Results and discussion

The powder x-ray diffraction (PXRD) patterns of Sm_2O_3 calcined at two different temperatures are presented in Figure 1. The PXRD pattern of Sm_2O_3-500 shows sharp peaks at 28.29 (222), 32.70 (044), 42.22 (431), 47.04 (440) and 55.74 (622), which demonstrates the pure cubic phase of the sample (JCPDS 15-0813) shown in Figure 1(a) [15]. Figure 1(b) displays the PXRD peaks for Sm_2O_3-700 and the most intense peaks are at 28.55 (222), 33.02 (044), 42.35 (431), 47.10 (440) and 56.04 (622), which signify the cubic crystal structure of the material (JCPDS 15-0813) [3]. The XRD patterns of the samples are fit accorded with the cubic crystal structure reported in Sm_2O_3 literature [15, 17]. From the Le-Bail refinement of XRD data, both samples exhibit a lattice parameter is 10.9 Å. Unlike Sm_2O_3-500, peaks of XRD data for Sm_2O_3-700 are sharper and more intense, indicating higher crystallinity of Sm_2O_3-700 sample [15]. XRD results show an increase in crystallinity with increasing calcination temperature, as well as peaks become sharper. The sharpness of the peaks is due to the larger size of the crystallites. Therefore, the crystallite size of the samples has been calculated using Debye-Scherrer's equation given below,

$$\text{Crystallite size (D)} = \frac{K\lambda}{\beta\cos\theta}$$

where D is known as the crystallite size, K is the Scherrer constant, λ is the X-ray wavelength, β is the full width at half maximum, and θ is the Bragg angle [15, 18, 19]. The obtained crystallite size for Sm_2O_3-500 is 16 nm, whereas for Sm_2O_3-700 it is 23 nm.

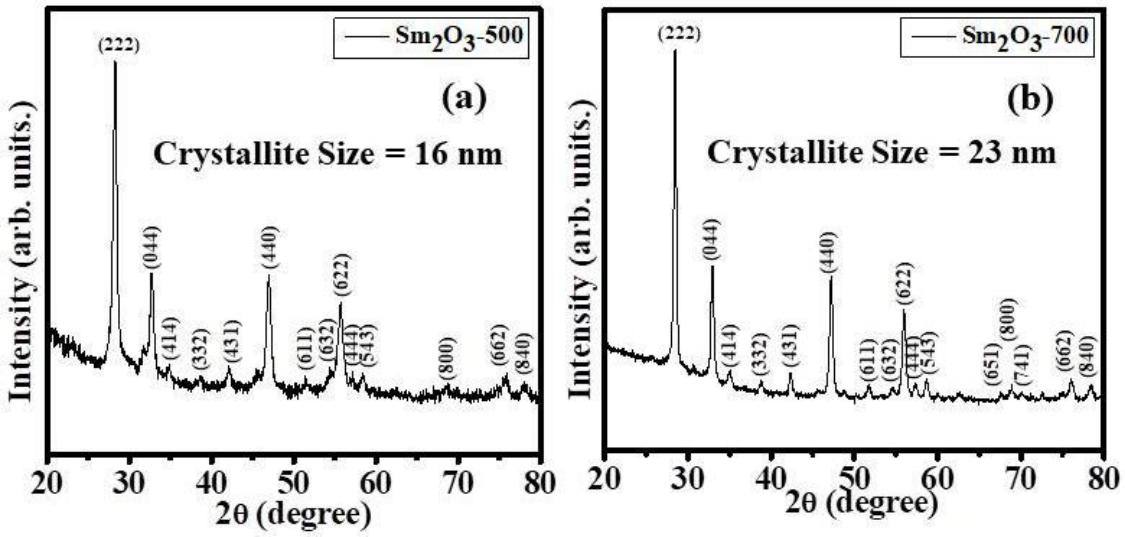

Figure 1: XRD pattern of the sample (*a*) Sm_2O_3-500 and (*b*) Sm_2O_3-700.

FTIR spectra of both the Sm_2O_3 samples are presented in Figure 2. The FTIR absorption spectrum for Sm_2O_3-500 and Sm_2O_3-700 is nearly the same shown in Figure 2 (a) and Figure 2 (b), respectively. Both of the samples show the characteristic absorption bands of pure Sm_2O_3 crystals located at around 456, 548 and 740 cm^{-1}, which correspond to Sm-O stretching vibrations [15, 16]. The results are well corroborated by the reported FTIR data [15, 16].

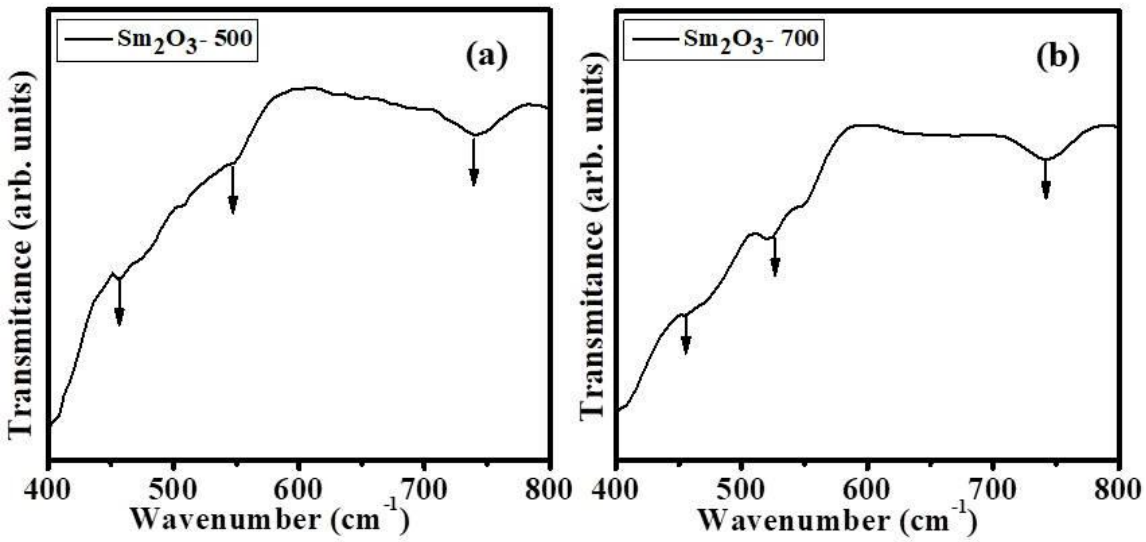

Figure 2: FTIR spectra of the sample (*a*) Sm_2O_3-500 and (*b*) Sm_2O_3-700.

Figure 3(a) and (b) exhibit the photocatalytic measurements of the synthesized samples, Sm_2O_3-500 and Sm_2O_3-700, respectively. Two containers having 50 ml of the aqueous solution of Methylene blue (MB), with 20 mg of two different samples of Sm_2O_3, that is, Sm_2O_3-500 and Sm_2O_3-700, have been carried out for photocatalytic analysis, respectively. Initially, without irradiation of UV radiation, UV-Visible measurements were performed, and an absorbance peak at 310.65 nm was obtained, which is the characteristic peak of MB. Then, for up to 20 minutes, the irradiation was carried out. Gradually MB peak intensity decreases with increasing irradiation time, which indicates that with irradiation, the dye gets degraded. By using the following equation degradation efficiency has been calculated.

$$\text{Degradation Efficiency (in percentage)} = \frac{(C0-Ct)}{C0} \times 100$$

where C_0 is the initial concentration of the dye and C_t is the concentration of dye at the time, t [2, 4].

Finally, it has been found that after 20 min irradiation of UV light, Sm_2O_3-500 degrades only 19% of the dye shown in Figure 4(a). However, Figure 4 (b) demonstrates Sm_2O_3-700, degrades 33% of the MB dye in 20 min. Recently, Jeon et al. [2] have shown the photocatalytic studies with pure Gd_2O_3 nanoparticles. Rahul et al. [4] and Luo et al. [5] studied the photocatalytic properties of La_2O_3. Similarly, some reports show the photocatalytic properties of the rare earth metal oxide composite materials [6-11]. All these reports are performed the photocatalytic studies to degrade the organic pollutants. Therefore, in this report, the effect of calcination temperature on the photocatalytic characteristics of Sm_2O_3 nanoparticles has been studied. It is found that compared to a 500 ˚C calcined sample, a 700 ˚C calcined sample is more efficient for photocatalysis.

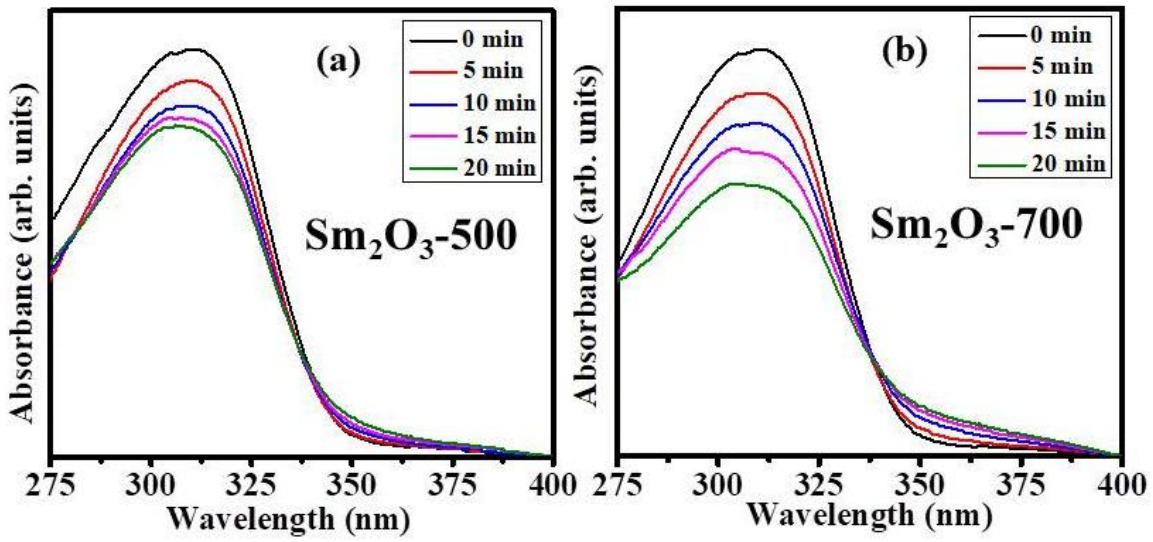

Figure 3: UV-Visible spectra of the MB dye with irradiation time (*a*) sample Sm_2O_3-500 and (*b*) sample Sm_2O_3-700.

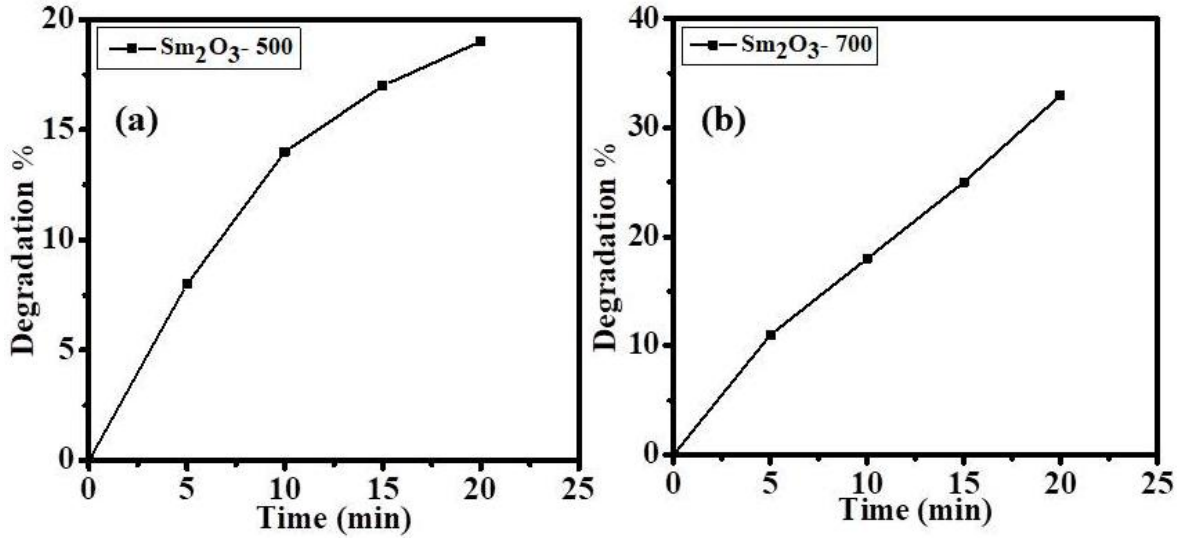

Figure 4: Dye degradation percentage (%) with irradiation time for the sample (a) Sm_2O_3-500 and (b) Sm_2O_3-700.

4 Conclusions

In this report, Sm_2O_3 nanoparticles were synthesized by the sol-gel technique. The synthesized sample was calcined at two different temperatures, which is 500 and 700 ˚C. Thereafter, the cubic crystal structure of the samples was confirmed by XRD. From the XRD data crystallite size of the samples was calculated. The obtained value of crystallite size for the Sm_2O_3-500 sample was 16 nm, whereas it was 23 nm for the sample Sm_2O_3-700. Both the samples exhibited Sm-O stretching vibrations confirmed from FTIR spectra. Photocatalytic analysis showed that Sm_2O_3-700 was more efficient under UV irradiation to degrade the dye MB.

Acknowledgments:

Financial support from the University of Johannesburg (UJ) GES is acknowledged. Prof Mallick and their research group are acknowledged for all the support for photocatalytic measurements.

References

[1] L. Yin, D. Wang, J. Huang, G. Tan, " Controllable synthesis of Sm_2O_3 crystallites with the assistance of tempelates by a hydrothermal calcination process," Materials Science in Semiconductor Processing, Vol. 30, pp. 9-13, 2015.

[2] S. Jeon, J-W. Ko, W-B. Ko, "Synthesis of Gd_2O_3 nanoparticles and their photocatalytic activity for degradation of azo dyes," Catalyst, Vol 11, pp. 742, 2021.

[3] M.M. Khan, S.N. Matussin, "Sm_2O_3 and Sm_2O_3-based nanostructures for photocatalysis, sensor, CO conversion, and biological applications," Catalysis Science and Technology, Vol. 13, pp. 2274, 2023.

[4] S. Rahul, G. Amal, R.S. Babu, A.D. Raj, G. Jayakumar, S.A. Rag, "Unraveling the photocatalytic performance of La_2O_3 nanoparticles for the degradation of six organic dyes," Langmuir, Vol. 41, pp. 16378-16390, 2025.

[5] X. Luo, L. Xu, L. Yang, J. Zhao, T. Asefa, R. Qiu, Z. Huang, "Ball milling of La_2O_3 tailors the crystal structure, reactive oxygen species, and free radical and non-free radical photocatalytic pathway," ACS Applied Materials and Interfaces, Vol.16, pp. 18671-18685, 2024.

[6] B. Subramanian, K.J. Jothi, M.M. Mohideen, R. Karthikeyan, A.S.K. Kumar, G.A. Sundaram, K. Thirumalai, M.D. Albaqami, S. Mohammad, M. Swaminathan, "Synthesis and characterization of

Dy_2O_3@TiO_2 nanocomposites for enhanced photocatalytic and electrocatalytic applications," ACS Engineering Au, Vol 4, pp. 474-490 2024.

[7] K. Jayaprakash, A. Sivasamy, "Superior photocatalytic performances of Dy_2O_3/graphitic cabon nitride nanohybrid for the oxidation of Rhodamine B dye under visible light irradiation: A superoxide free radicals approach," Colloids and Surfaces A: Physicochemical and Engineering Aspects, Vol. 676, pp. 132260, 2023.

[8] Y. Xie, J. Wu, C. Sun, Y. Ling, S. Li, X. Li, J. Zhao, K. Yang, "La_2O_3-modified graphite carbon nitride achieving the enhanced photocatalytic degradation of different organic pollutants under visible light irradiation," Materials Chemistry and Physics, Vol. 246, pp. 122846, 2020.

[9] Z. Zhu, H. Xia, R. Wu, Y. Cao, H. Li, "Fabrication of La_2O_3/g-C_3N_4 heterojunction with enhanced photocatalytic performance of tetracycline hydrochloride," Crystals, Vol. 11, pp. 1349, 2021.

[10] A. Marizcal-Barba, I. Limon-Rocha, A. Barrera, J.E. Casillas, O.A. Gonzalez-Vargas, J.L. Rico, C. Martinez-Gomez, A. Perez-Larios, "TiO_2-La_2O_3 as photocatalysts in the degradation of naproxen," Inorganics, Vol. 10, pp. 67, 2022.

[11] A. Barrera, F. Tzompantzi, J. Campa-Molina, J.E. Casillas, R. Perez-Hernandez, S. Ulloa-Godinez, C. Velasquez, J. Arenas-Alatorre, "Photocatalytic activity of Ag/Al_2O_3-Gd_2O_3 photocatalysts prepared by the sol-gel method in the degradation of 4-chlorophenol," RSC Advances, Vol. 8, pp. 3108, 2018.

[12] B. Bharati, N.C. Mishra, A.S.K. Sinha, C. Rath, "Unusual structural transformation and photocatalytic activity of Mndoped TiO_2 nanoparticles under sunlight," Materials Research Bulletin, Vol. 123, pp. 110710, 2020.

[13] B. Bharati, A.K. Sonkar, N. Singh, D. Dash, C. Rath, "Enhanced photocatalytic degradation of dyes under sunlight using biocompatible TiO_2 nanoparticle," Materials Research Express, Vol. 4, pp. 085503, 2017.

[14] M. Jourshabani, Z. Shariatinia, A. Badiei, " Synthesis and charaterisation of novel Sm_2O_3/S-doped g-C_3N_4 nanocomposites with enhanced photocatalytic activities under visible light irradiation," Applied Surface Science, Vol. 427, pp. 375-387, 2018.

[15] S. Biswas, H, Naskar, S. Pradhan, Y. Chen, Y. Wang, Rajib Bandyopadhyay, Panchanan Pramanik, "Sm_2O_3 nanorod-modified graphite paste electrode for trace level voltammetric determination of acetaminophen and ciprofloxacin," New J. Chemistry Vol. 44, pp. 1921, 2020.

[16] B.T. Sone, E. Manikandan, A. Gurib-Fakim, M. Maaza, "Sm_2O_3 nanoparticles green synthesis via callistemon viminalis' extract," Journal of Alloys and Compounds, Vol. 650, pp. 357-362, 2015.

[17] H.M. Shiri, A. Ehsani, M.J. Khales, "Electrochemical synthesis of Sm_2O_3 nanoparticles: application in conductive polymer composite films for supercapacitor," Journal of Colloid and Interface Science, Vol. 505, pp. 940-946, 2017.

[18] K.H. Goh, A.S.M.A. Haseeb, Y.H. Wong, "Physical and electrical properties of thermal oxidized Sm_2O_3 gate oxide thin film on Si Substrate: influence of oxidation durations," Thin Solid Films, Vol. 606, pp. 80-86, 2016.

[19] S.R. Jamnani, H.M. Moghaddam, S.G. Leonardi, G. Neri, "A novel conductometric sensor based on hierarchical self-assembly nanoparticles Sm_2O_3 for VOCs monitoring," Ceramic International, Vol. 44, pp. 16953-16959, 2018.